NIA Computational Fluid Dynamics Seminar
Hampton VA, June 19, 2013

Adjoint-based Optimization of Flapping Wing Flows

Martin Jones *and* *Nail Yamaleev*

North Carolina A&T State University

Acknowledgements

This work was partially supported by Army Research Laboratory (ARL) Grant W911NF-08-2-0004.

Outline

- Motivation
- Governing equations
- Numerical method
- Time-dependent optimization problem
- Adjoint-based methodology
- Wing kinematics and shape parameterization
- Optimization results
  - Optimization of wing shape
  - Optimization of wing kinematics
  - Combined optimization of shape and kinematics
- Conclusions
- Future directions

Motivation

- Replicating the wing kinematics and shape of flying insects is not enough for designing efficient MAVs.
- State-of-the-art materials, micro-scale actuators, propulsion systems, and power sources are less efficient than those created by Mother Nature.
- Different region of the design space has to investigated.

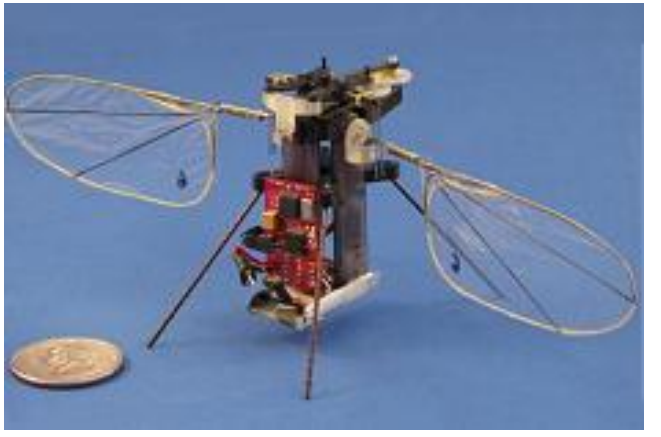

Flapping-wing MAV

A bee mitigating a gust.

Technical Challenges

- Highly unsteady, vortex-dominated, low-Reynolds-number flows.
- Complex geometry and wing kinematics.
- Wing-wake interaction and vortex shedding.
- Fluid/structure interaction with large deformations.
- Unsteady laminar-turbulent transition and relaminarization.

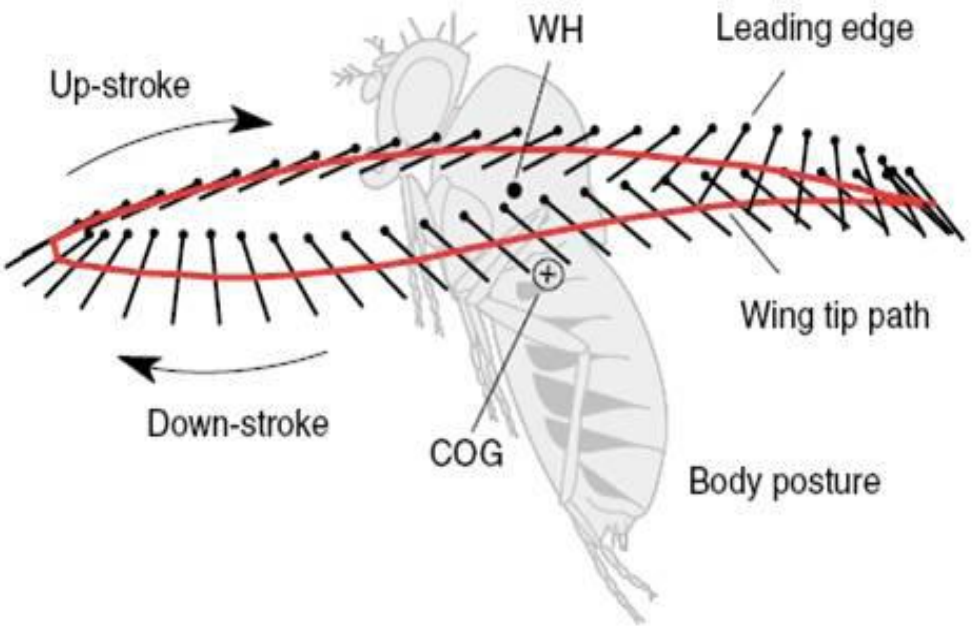

Computational Challenges

- Resolution of multiple temporal and spatial scales.
- Very large number of design variables
- Multiple solves of the 3-D unsteady Navier-Stokes and adjoint equations on moving grids.
- Nonlinear dependence of the MAV performance on the input parameters/design variables
- Large storage and computational costs.
- Transition prediction
- Strong CFD/CSD coupling

Governing Equations

The 3-D unsteady incompressible Reynolds-averaged Navier-Stokes equations on moving and deforming control volume

$$\frac{\partial (V\mathbf{Q})}{\partial t} + \oint_{\Gamma} (\mathbf{F}_{in} - \mathbf{F}_{v}) \cdot \mathbf{n} d\Gamma = \mathbf{0}$$

$$\mathbf{F}_{in} = \begin{bmatrix} \beta(u - W_x) \\ u(u - W_x) + p \\ v(u - W_x) \\ w(u - W_x) \end{bmatrix} \mathbf{i} + \begin{bmatrix} \beta(v - W_y) \\ u(v - W_y) \\ v(v - W_y) + p \\ w(v - W_y) \end{bmatrix} \mathbf{j} + \begin{bmatrix} \beta(w - W_z) \\ u(w - W_z) \\ v(w - W_z) \\ w(w - W_z) + p \end{bmatrix} \mathbf{k}$$

$W_x,\ W_y,\ W_z$ – x, y, z components of the local face velocity vector

For special case ***Q***=*const*, the governing equations reduce to GCL

$$\frac{\partial V}{\partial t} + \oint_{\Gamma} \mathbf{W} \cdot \mathbf{n} d\Gamma = \mathbf{0}$$

Rigidly Moving Grids

Rigid grid motion is defined in the matrix form

$$\mathbf{x} = T\mathbf{x}_0$$

$$\begin{bmatrix} x \\ y \\ z \\ 1 \end{bmatrix} = \begin{bmatrix} \boldsymbol{r_{11}} & \boldsymbol{r_{12}} & \boldsymbol{r_{13}} & t_1 \\ \boldsymbol{r_{21}} & \boldsymbol{r_{22}} & \boldsymbol{r_{23}} & t_2 \\ \boldsymbol{r_{31}} & \boldsymbol{r_{32}} & \boldsymbol{r_{33}} & t_3 \\ 0 & 0 & 0 & 1 \end{bmatrix} \begin{bmatrix} x_0 \\ y_0 \\ z_0 \\ 1 \end{bmatrix}$$

R – 3x3 rotation matrix, **t** – translation vector

For multiple transformations $T = T_1 T_2 T_3 \ldots$

Grid equation:

$$\mathbf{G}^n(\mathbf{X}^n, \mathbf{X}^0, \mathbf{D}) \equiv \mathbf{R}\ {}^n\mathbf{X}^0 + \boldsymbol{\tau}^n - \mathbf{X}^n$$

where

$\mathbf{R} \equiv$ matrix of 3x3 blocks specifying rotations

$\boldsymbol{\tau} \equiv$ vector of 3x1 blocks specifying translations

Flow/Adjoint Solver

FUN3D: Fully Unstructured 3D RANS code

- **Temporal discretization**
  - Dual time stepping technique
  - Implicit 2nd-order BDF scheme
- **Spatial discretization**
  - 2nd-order, node-centered FV discretization for the inviscid terms
  - 2nd-order Galerkin discretization for the viscous terms
  - Roe-flux splitting (with no limiters)
- **Unstructured moving grids**
  - Geometric conservation law terms
  - Rigidly moving grids
- **Turbulence models**: Spalart-Allmaras turbulence model
- **Highly scalable MPI implementation using domain decomposition**
- **Time-dependent adjoint-based optimization**

Discrete Time-Dependent Optimization Problem

Find the design D and flow Q variables such that

$$\begin{cases} \min\limits_{\mathbf{D}\in\mathcal{D}_a} F_{\text{obj}}(\mathbf{D}); \quad F_{\text{obj}} = \sum\limits_{n=0}^{N} f^n(\mathbf{Q}^n, \mathbf{X}^n, \mathbf{D})\Delta t \\ \text{subject to}: V^n \dfrac{\mathbf{Q}^n - \mathbf{Q}^{n-1}}{\Delta t} + \mathbf{R}(\mathbf{Q}^n, \mathbf{X}^n, \mathbf{D}) + \boldsymbol{R}_{GCL}\mathbf{Q}^{n-1} = 0 \\ \mathbf{G}^n(\mathbf{X}^0, \mathbf{X}^n, \mathbf{D}) = 0 \end{cases}$$

Objective functional: $$f^n = \sum_{j=1}^{J} \omega_j \left[C_j^n - \left(C_j^{\text{target}} \right)^n \right]^2$$

Geometric Conservation Law: $$\frac{V^n - V^{n-1}}{\Delta t} = \boldsymbol{R}_{GCL}^n$$

Adjoint-based Methodology

Lagrangian functional:

$$L(\mathbf{Q},\mathbf{X},\mathbf{D},\boldsymbol{\Lambda}_f,\boldsymbol{\Lambda}_g)=\sum_{n=1}^{N} f^n\Delta t+\sum_{n=1}^{N}\left[\boldsymbol{\Lambda}_f^n\right]^T\left(V^n\frac{\mathbf{Q}^n-\mathbf{Q}^{n-1}}{\Delta t}+\mathbf{R}^n+\boldsymbol{R}_{GCL}^n\mathbf{Q}^{n-1}\right)\Delta t$$
$$+\sum_{n=1}^{N}\left[\boldsymbol{\Lambda}_g^n\right]^T\mathbf{G}^n\Delta t$$

Differentiating L with respect to D yields:

$$\frac{dL}{d\mathbf{D}}=\sum_{n=1}^{N}\left(\frac{\partial f^n}{\partial\mathbf{D}}+\left[\boldsymbol{\Lambda}_f^n\right]^T\left(\frac{\partial\mathbf{R}^n}{\partial\mathbf{D}}+\frac{\partial\boldsymbol{R}_{GCL}{}^n}{\partial\mathbf{D}}\mathbf{Q}^{n-1}\right)+\left[\boldsymbol{\Lambda}_g^n\right]^T\frac{\partial\mathbf{G}^n}{\partial\mathbf{D}}\right)\Delta t$$

$$+\sum_{n=1}^{N}\left(\frac{V^n\boldsymbol{\Lambda}_f^n-V^{n+1}\boldsymbol{\Lambda}_f^{n+1}}{\Delta t}+\left[\frac{\partial\mathbf{R}^n}{\partial\mathbf{Q}^n}\right]^T\boldsymbol{\Lambda}_f^n+\boldsymbol{R}_{GCL}^n\boldsymbol{\Lambda}_f^{n+1}+\left[\frac{\partial f^n}{\partial\mathbf{Q}^n}\right]^T\right)^T\frac{\partial\mathbf{Q}^n}{\partial\mathbf{D}}\Delta t$$

$$+\sum_{n=1}^{N}\left(\left[\frac{\partial\mathbf{G}^n}{\partial\mathbf{X}^n}\right]^T\boldsymbol{\Lambda}_g^n+\left[\frac{\partial V^n}{\partial\mathbf{X}^n}\frac{\mathbf{Q}^n-\mathbf{Q}^{n-1}}{\Delta t}\right]^T\boldsymbol{\Lambda}_f^n+\sum_{k=0}^{1}\left[\frac{\partial\mathbf{R}^{n+k}}{\partial\mathbf{X}^n}+\frac{\partial\boldsymbol{R}_{GCL}^{n+k}}{\partial\mathbf{X}^n}\mathbf{Q}^{n+k-1}\right]^T\boldsymbol{\Lambda}_f^{n+k}+\left[\frac{\partial f^n}{\partial\mathbf{X}^n}\right]^T\right)^T\frac{\partial\mathbf{X}^n}{\partial\mathbf{D}}\Delta t$$

Adjoint-based Methodology (cont.)

Flow adjoint equations:

$$\frac{V^n \boldsymbol{\Lambda}_f^n - V^{n+1}\boldsymbol{\Lambda}_f^{n+1}}{\Delta t} + \left[\frac{\partial \mathbf{R}^n}{\partial \mathbf{Q}^n}\right]^T \boldsymbol{\Lambda}_f^n + \boldsymbol{R}_{GCL}^n \boldsymbol{\Lambda}_f^{n+1} = -\left[\frac{\partial f^n}{\partial \mathbf{Q}^n}\right]^T$$

Grid adjoint equation:

$$\left[\frac{\partial \mathbf{G}^n}{\partial \mathbf{X}^n}\right]^T \boldsymbol{\Lambda}_g^n = -\left[\frac{\partial V^n}{\partial \mathbf{X}^n}\frac{\mathbf{Q}^n - \mathbf{Q}^{n-1}}{\Delta t}\right]^T \boldsymbol{\Lambda}_f^n - \sum_{k=0}^{1}\left[\frac{\partial \mathbf{R}^{n+k}}{\partial \mathbf{X}^n} + \frac{\partial \boldsymbol{R}_{GCL}^{n+k}}{\partial \mathbf{X}^n}\mathbf{Q}^{n+k-1}\right]^T \boldsymbol{\Lambda}_f^{n+k} - \left[\frac{\partial f^n}{\partial \mathbf{X}^n}\right]^T$$

1. The same adjoint equations can be used *regardless of the number of the control variables* $\boldsymbol{D}$!
2. The adjoint equations are integrated *backward in time*.
3. The *flow solutions for all time levels must be available* to integrate the adjoint equations!

Adjoint-based Methodology (cont.)

Sensitivity derivative:

$$\frac{dL}{d\mathbf{D}} = \sum_{n=0}^{N} \left(\frac{\partial f^{n}}{\partial \mathbf{D}} + \left[\mathbf{\Lambda}_{f}^{n} \right]^{T} \left(\frac{\partial \mathbf{R}^{n}}{\partial \mathbf{D}} + \frac{\partial \mathbf{R}_{GCL}^{n}}{\partial \mathbf{D}} \mathbf{Q}^{n-1} \right) + \left[\mathbf{\Lambda}_{g}^{n} \right]^{T} \frac{\partial \mathbf{G}^{n}}{\partial \mathbf{D}} \right) \Delta t$$

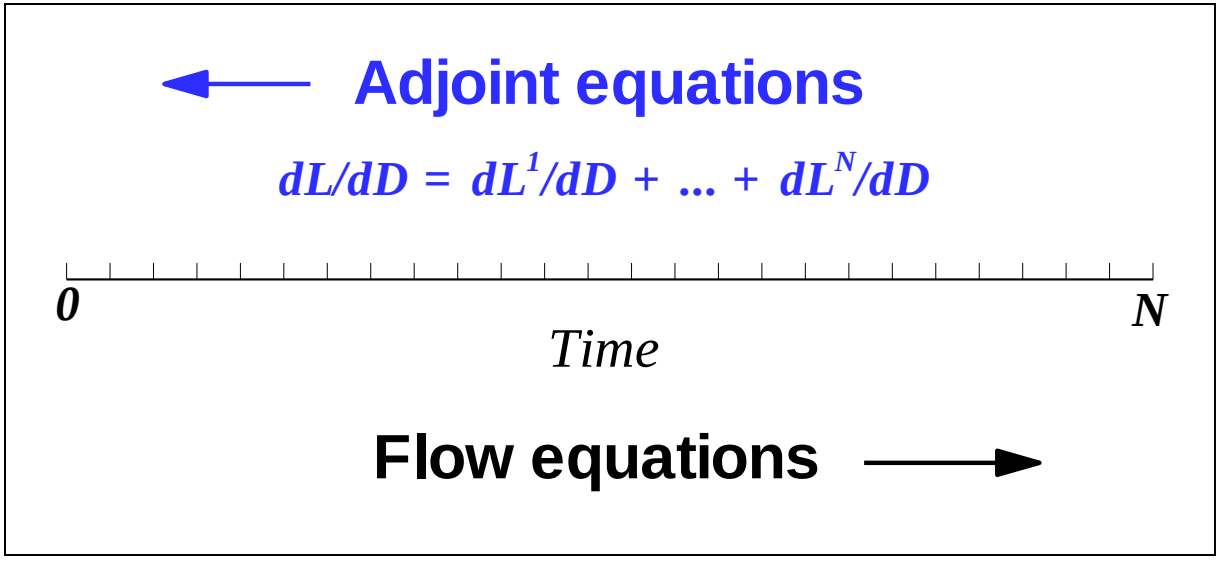

Wing kinematics

$$\begin{cases} \theta = \sum_{k=1}^{s} \theta_k P_k^{\theta}(f_\theta, t) \\ \alpha = \sum_{k=1}^{s} \alpha_k P_k^{\alpha}(f_\alpha, t) \\ \varphi = \sum_{k=1}^{s} \varphi_k P_k^{\varphi}(f_\varphi, t) \end{cases}$$

θ -stroke angle

α - pitch angle

φ - heave angle

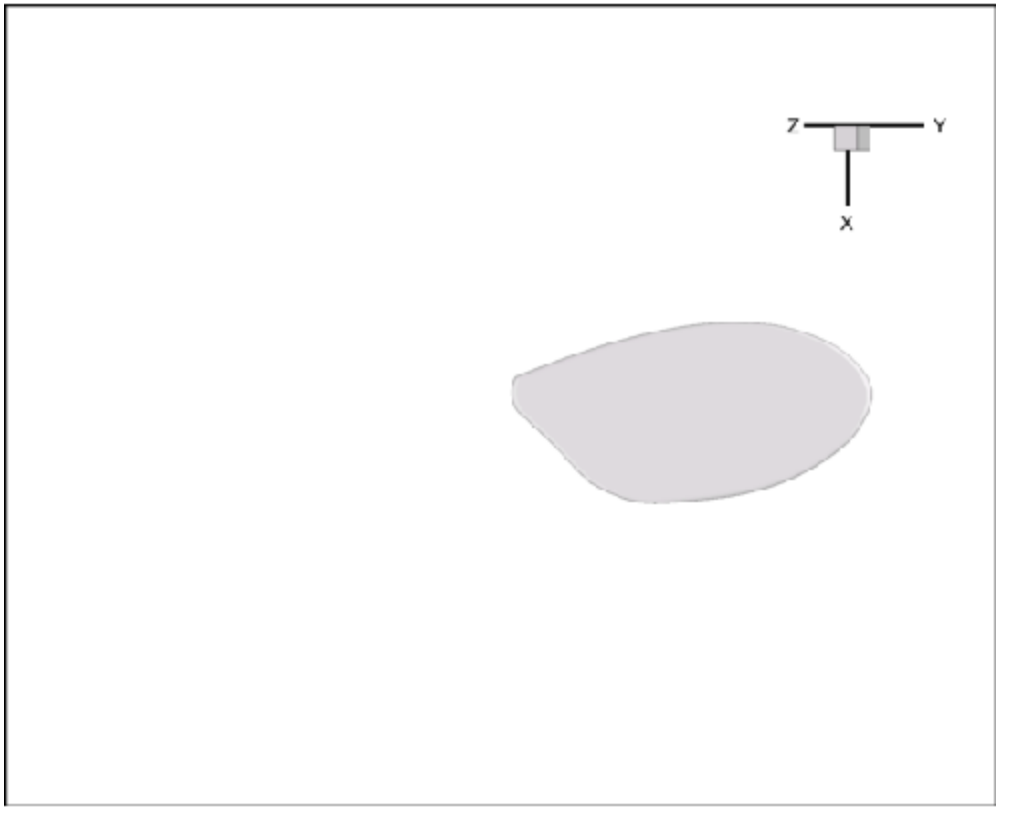

Frequencies are defined by $f_\theta = f_\alpha = f, \quad f_\varphi = 2f$

Selecting a proper design space for kinematics variables is not a trivial problem!

Geometry Parameterization

MASSOUD is used for wing surface parameterization

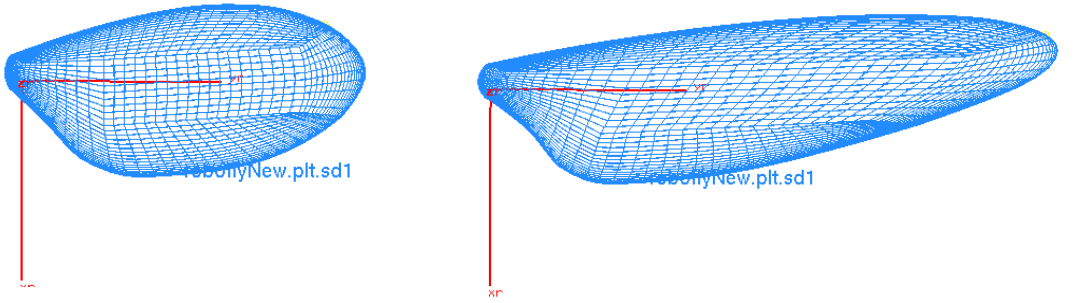

Wing planform

<u>Shape design variables:</u>

12 planfrom variables

7 twist variables

Thinning is not allowed

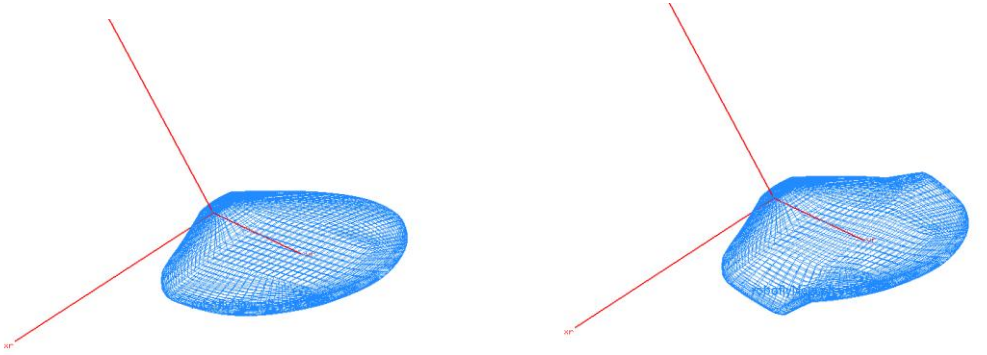

Wing twist

Computational details

- One desktop Dell workstation with dual-socket quad-core 2.4 GH Nehalem processor, 24 Gb RAM.
- Hexahedral grid with 251,766 nodes
- BDF2 was used with 30 - 40 subiterations at each time step.
- 100 - 150 time steps were used per each flapping cycle.
- Individual flow and adjoint solutions require about 4 h of wall-clock time each.
- 4-6 GB of disk space is required to store the entire flow solution.
- Total computational time is 3.5 – 6 days

Optimization Results

Case 1: Optimization of wing geometry

Case 2: Optimization of wing kinematics

Case 3: Combined optimization of wing shape and kinematics using the same design variables as in Cases 1 and 2

Reynolds number: Re=2000

Baseline reduced frequency: f =0.236

Baseline amplitudes: $\theta_0 = 60^0,\ \alpha_0 = 45^0,\ \varphi_0 = 0^0$

Objective functional: $f^n = \left(C_x^n - C_{\text{target}}^n\right)^2 + \omega_1\left(C_y^n\right)^2 + \omega_2\left(C_z^n\right)^2$

19 shape design variables (12 planform, 7 twist variables)

8 kinematic variables

Case 1: Optimization of wing shape

Optimization of wing shape

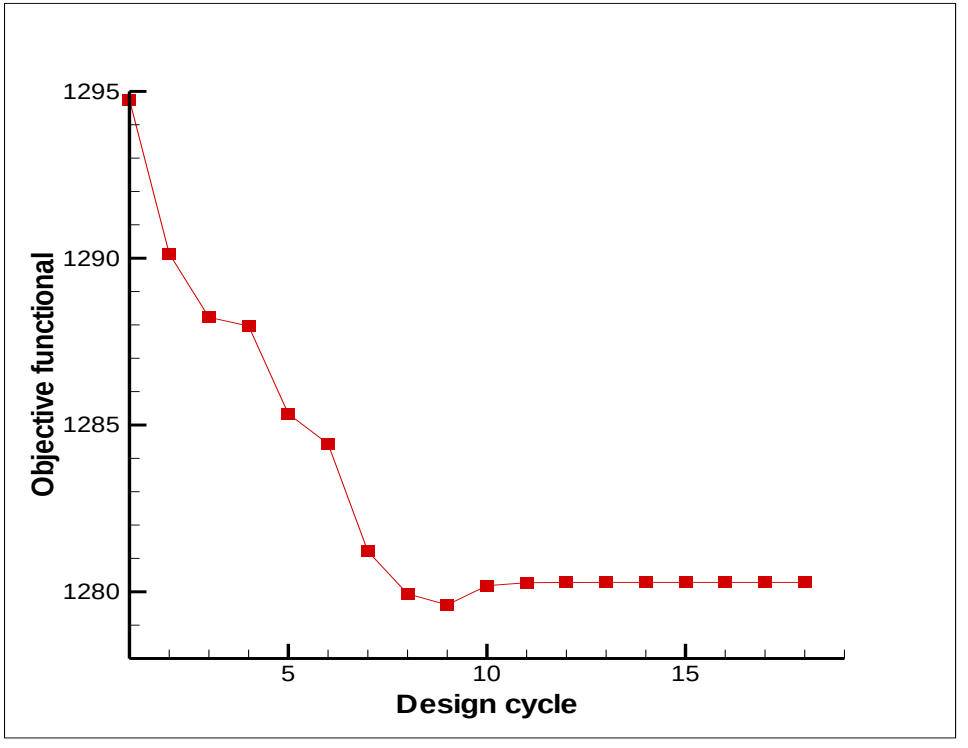

Convergence history of the objective functional

Optimization of wing shape

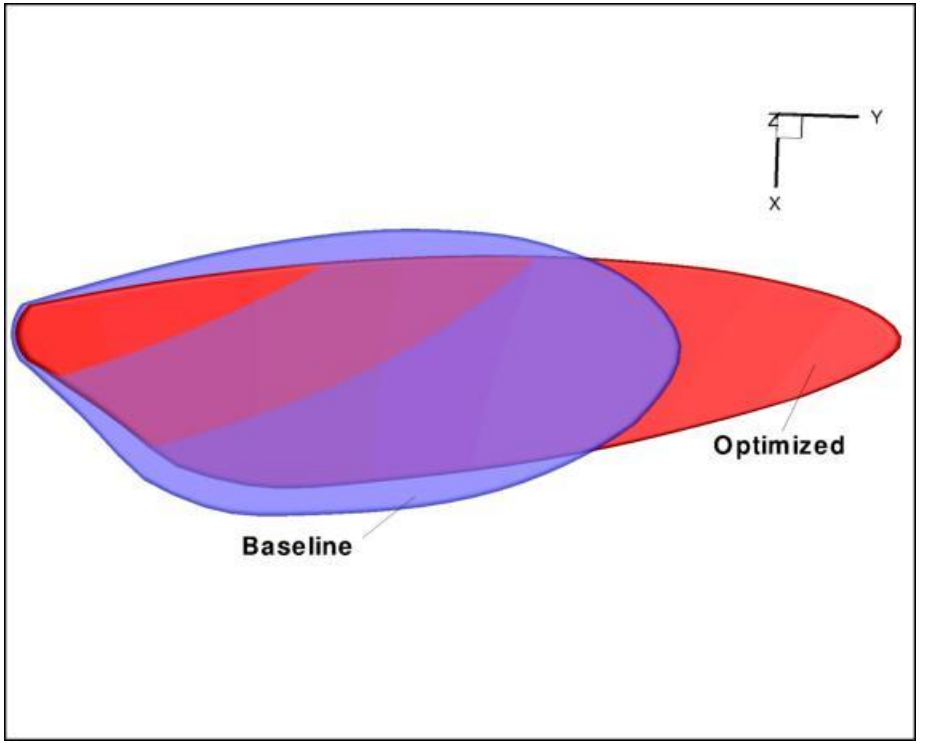

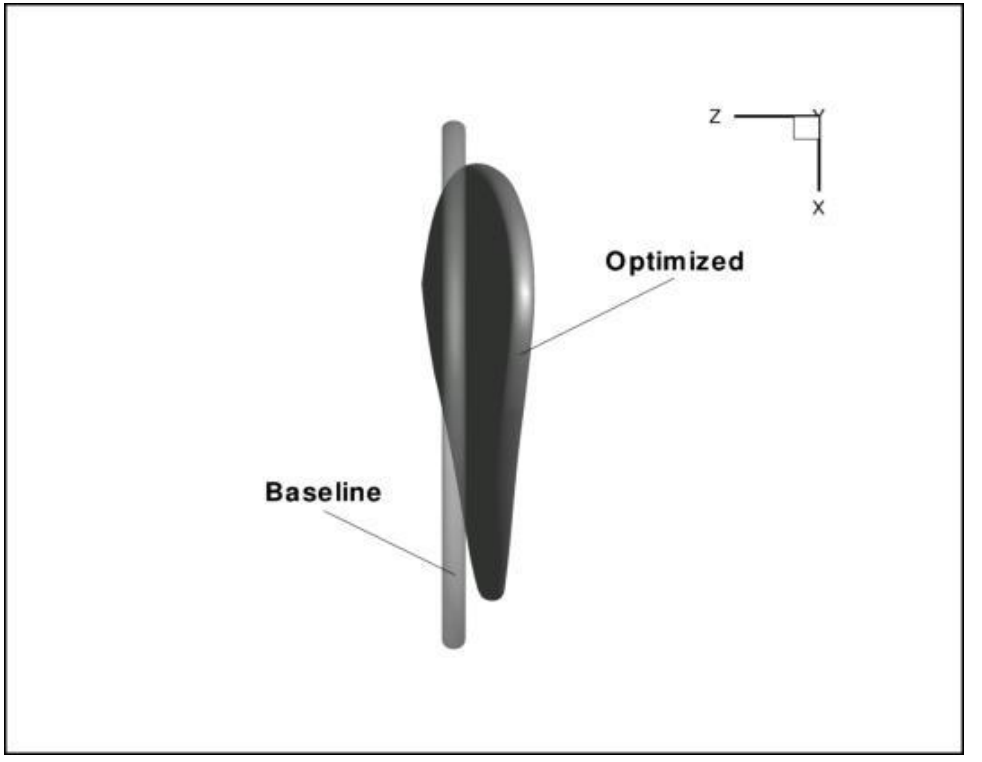

Baseline and optimized wing geometries

Optimization of wing shape (cont.)

Baseline **Optimal**

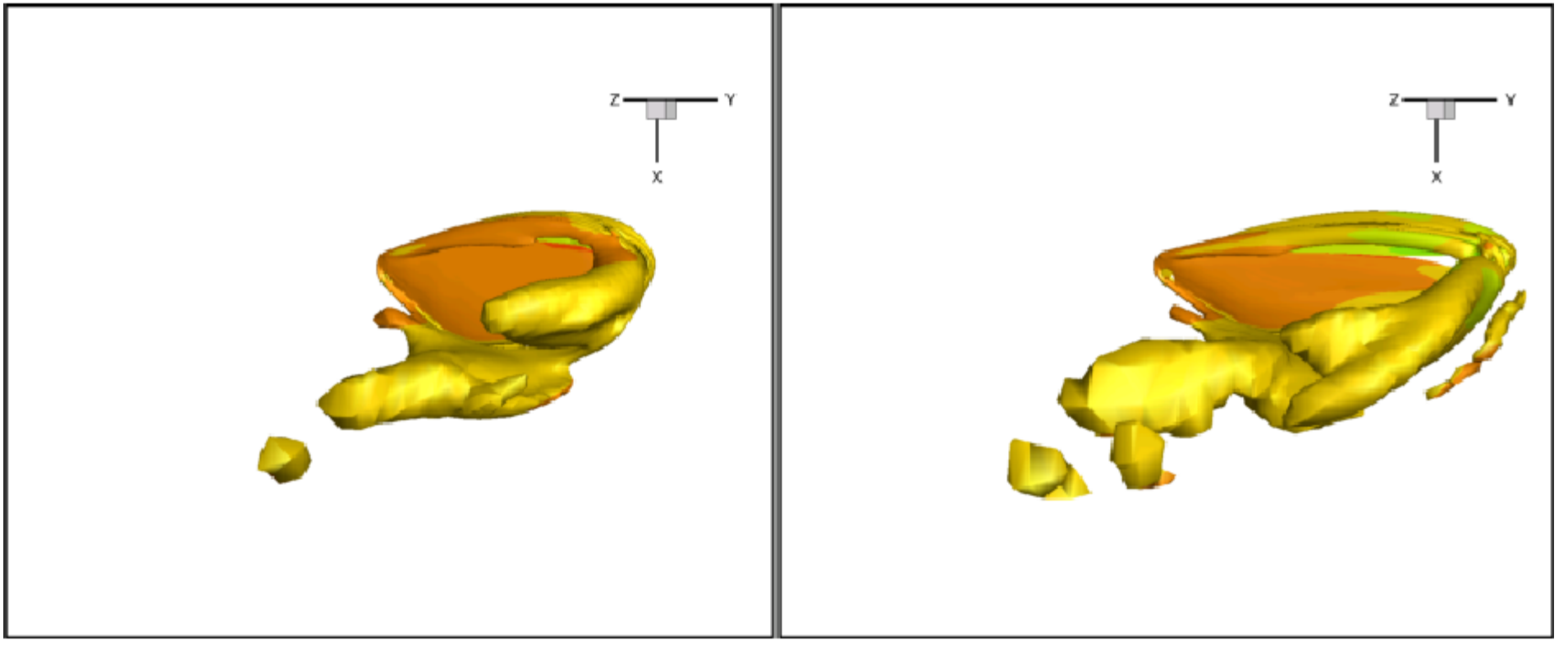

Iso-surface of the *q*-criterion colored with pressure contours obtained with the baseline (left) and optimized wing geometry.

Optimization of wing shape (cont.)

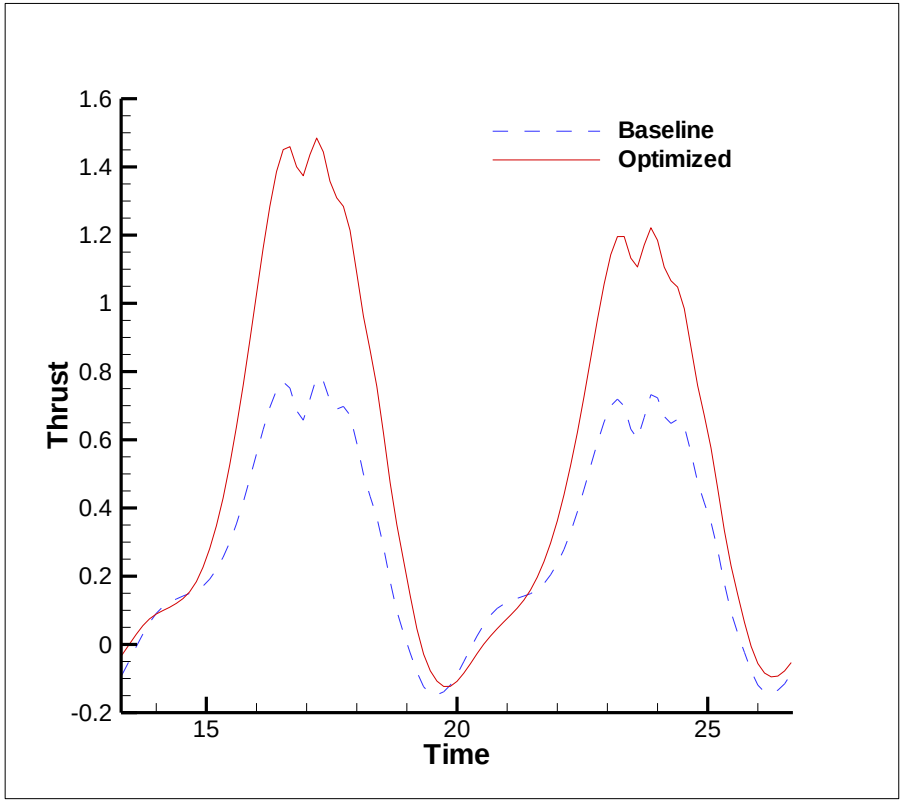

Baseline and optimized thrust coefficients.

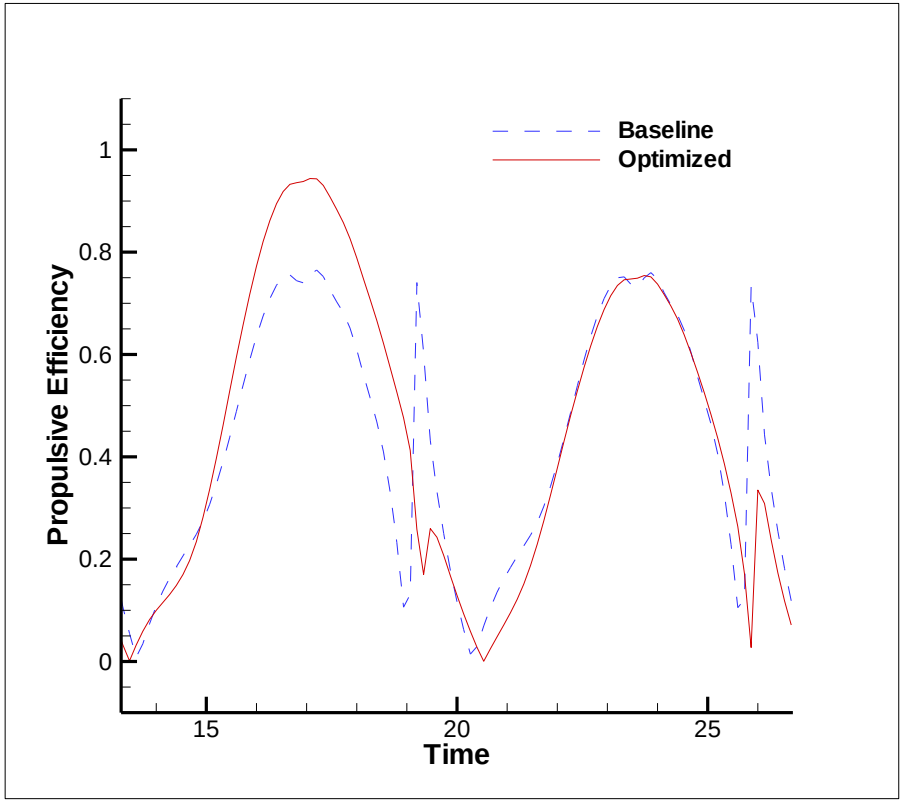

Propulsive efficiency before and after optimization.

Case 2: Optimization of wing kinematics

Optimization of wing kinematics

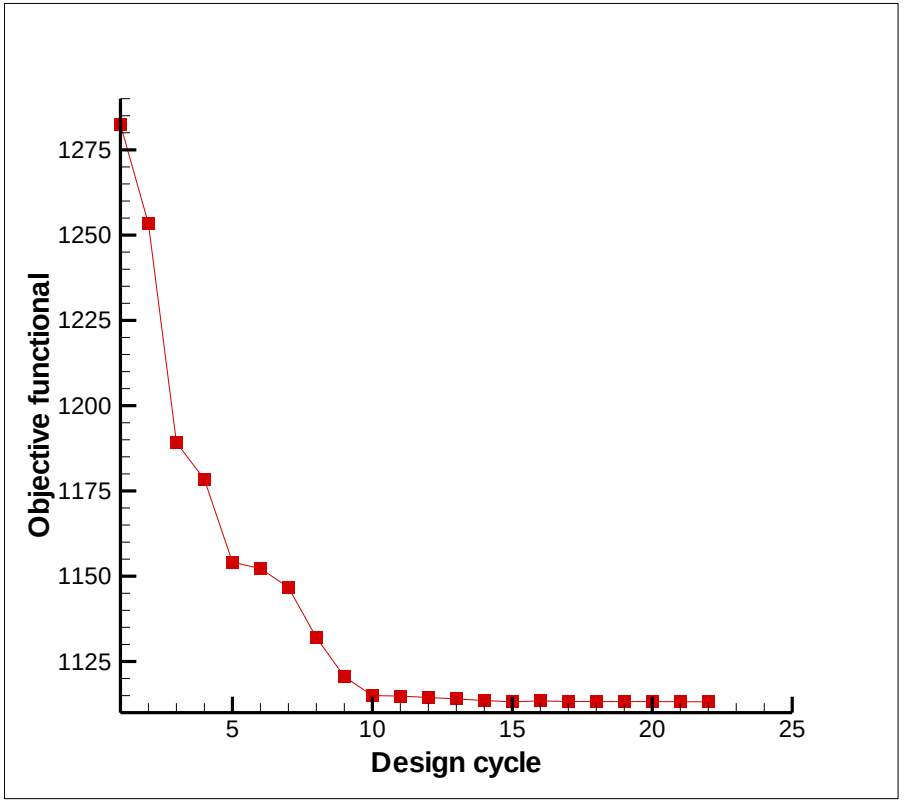

Convergence history of the objective functional

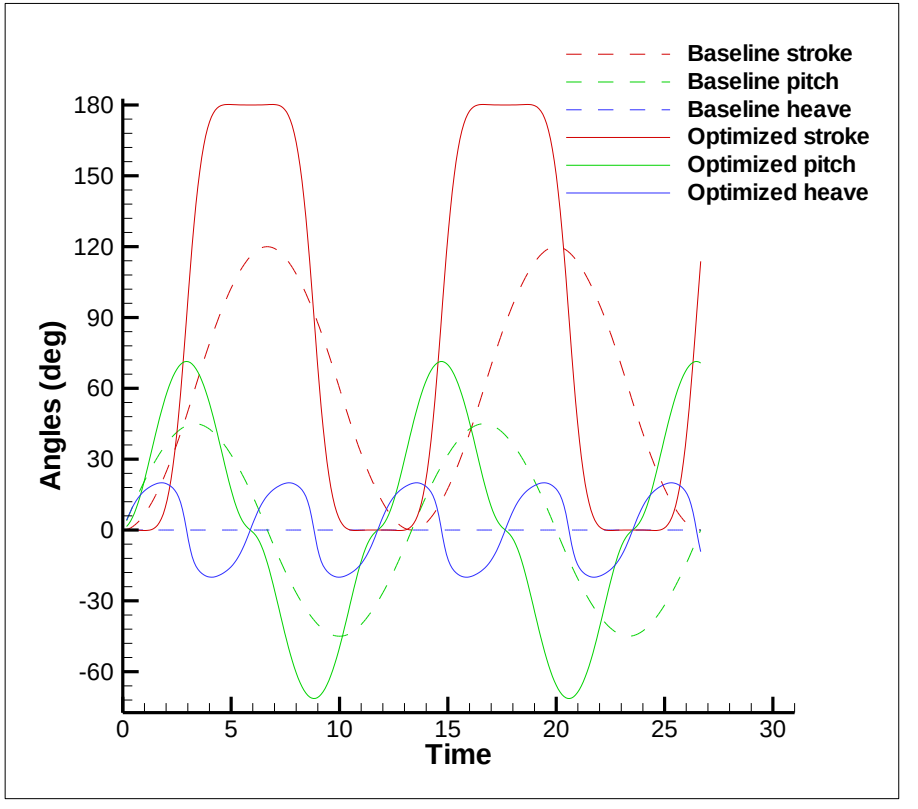

Baseline and optimized stroke pitch and heave angle profiles

Optimization of wing kinematics (cont.)

Baseline **Optimal**

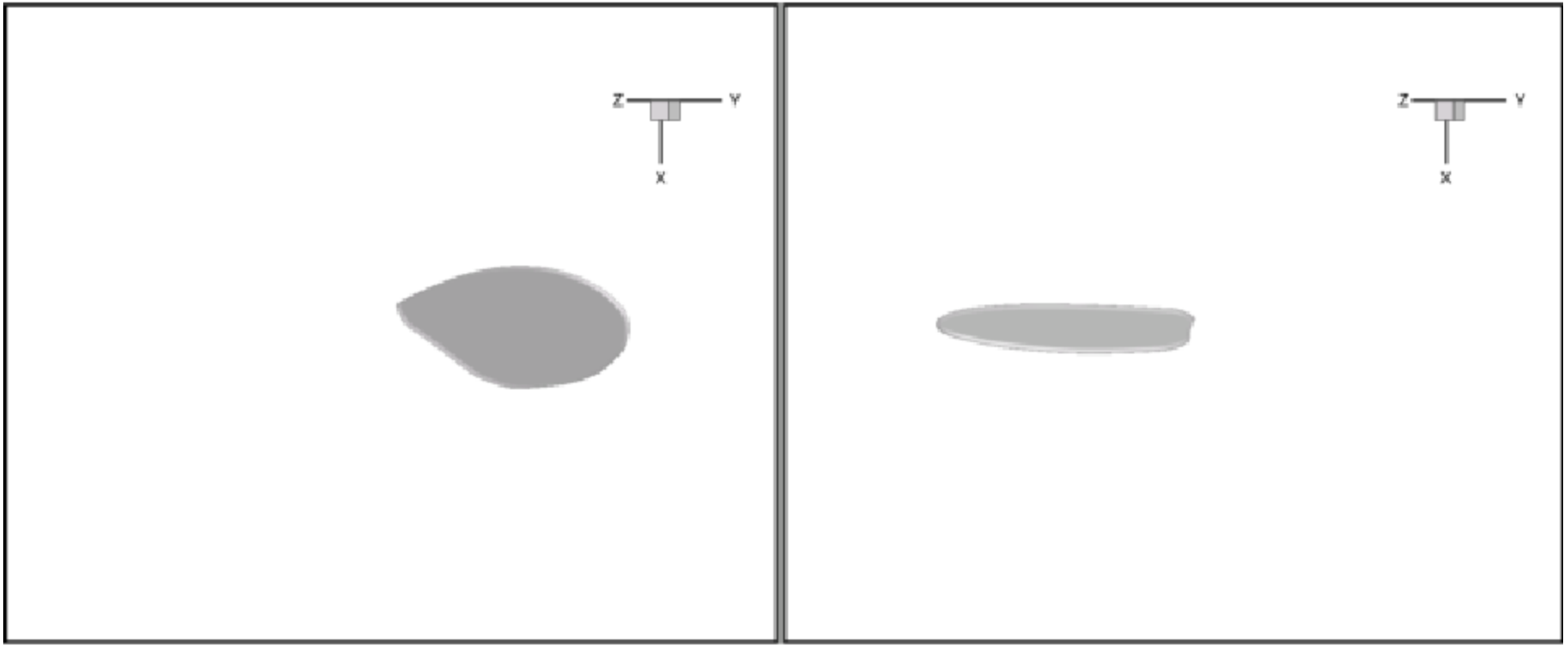

The baseline (left) and optimized wing kinematics.

Optimization of wing kinematics (cont.)

Baseline **Optimal**

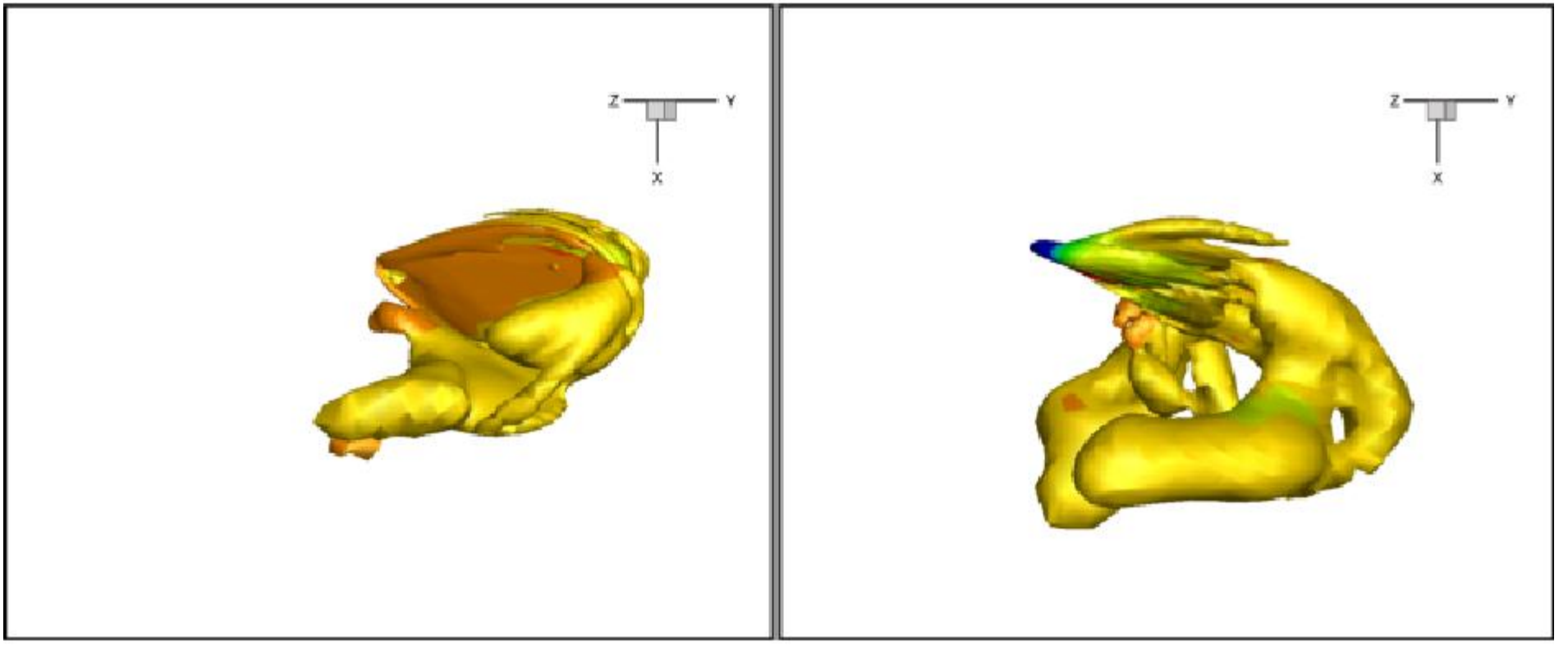

Iso-surface of the *q*-criterion colored with pressure contours obtained with the baseline (left) and optimized wing kinematics.

Optimization of wing kinematics (cont.)

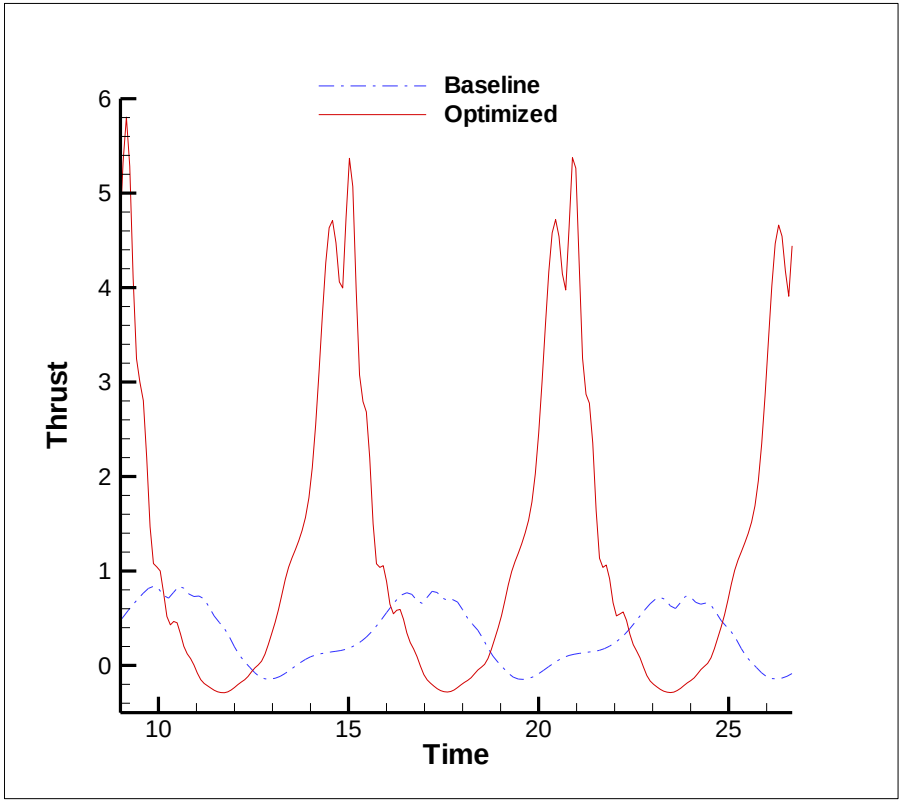

Baseline and optimized thrust coefficients.

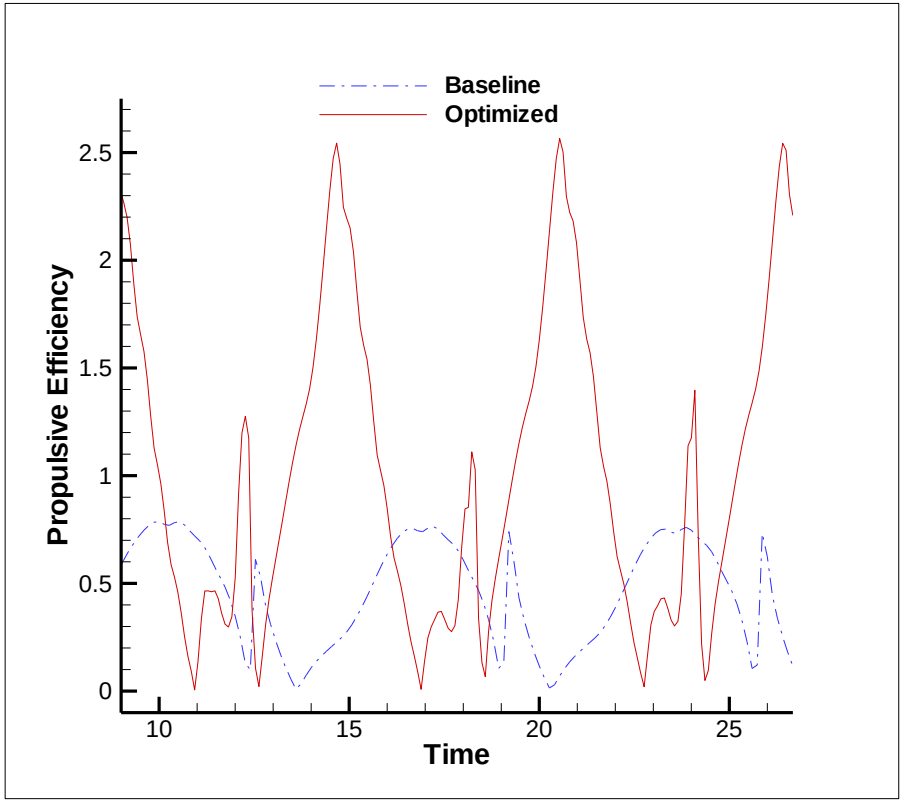

Propulsive efficiency before and after optimization.

Case 3: Combined Optimization of wing shape and kinematics

Combined Optimization of wing shape and kinematics

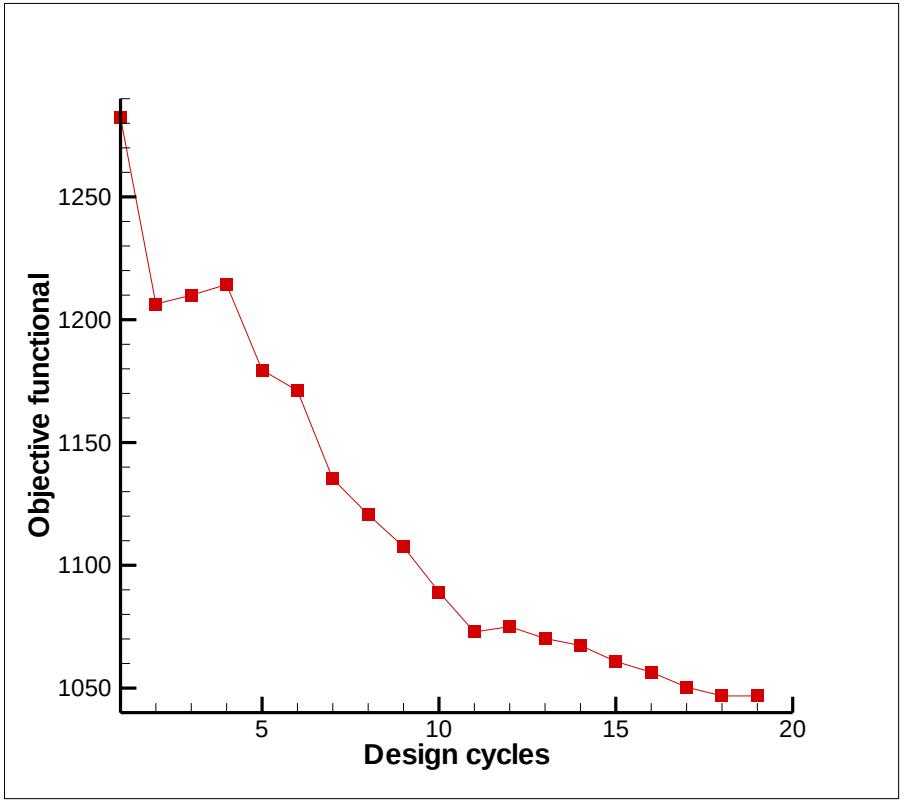

Convergence history of the objective functional

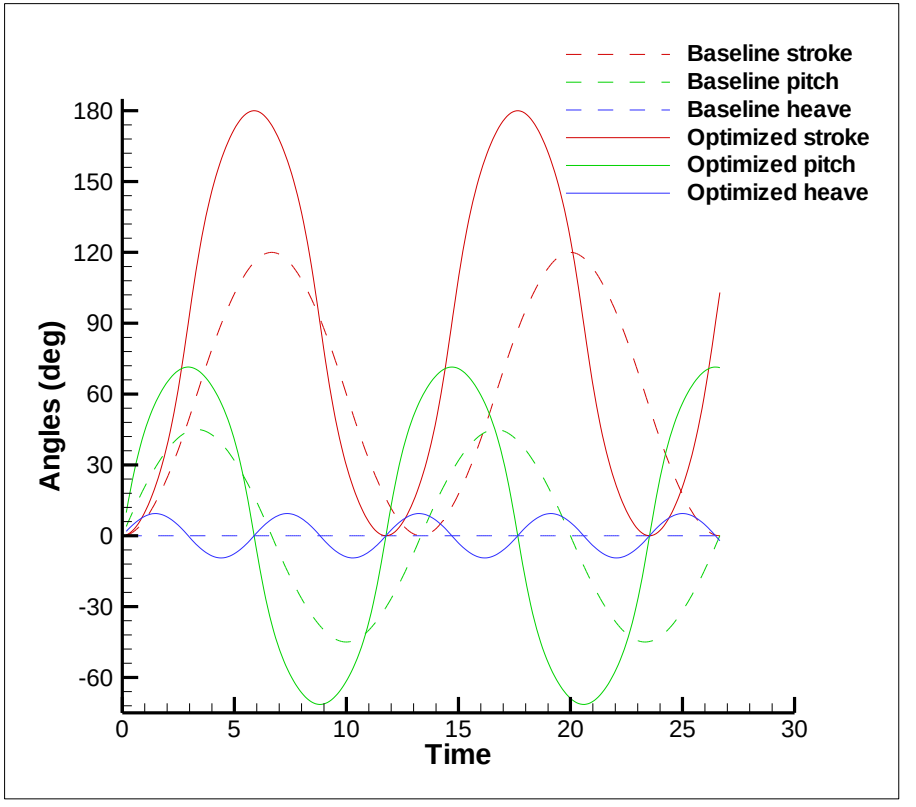

Baseline and optimized stroke, pitch, and heave angle profiles

Combined Optimization of wing shape and kinematics

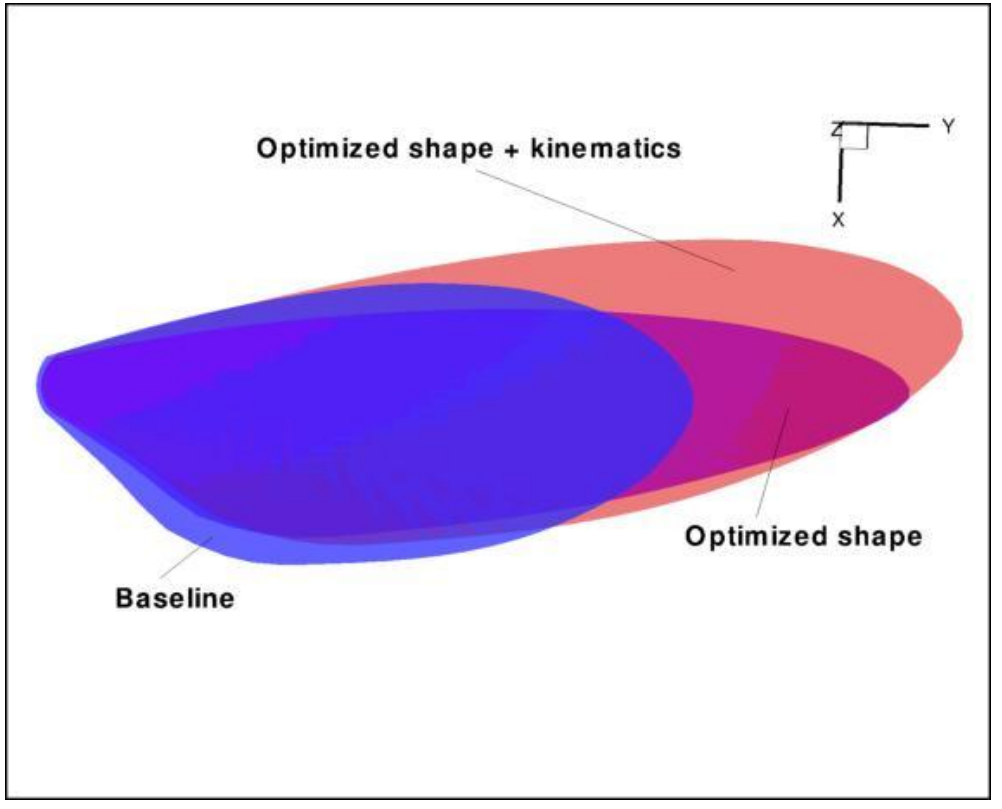

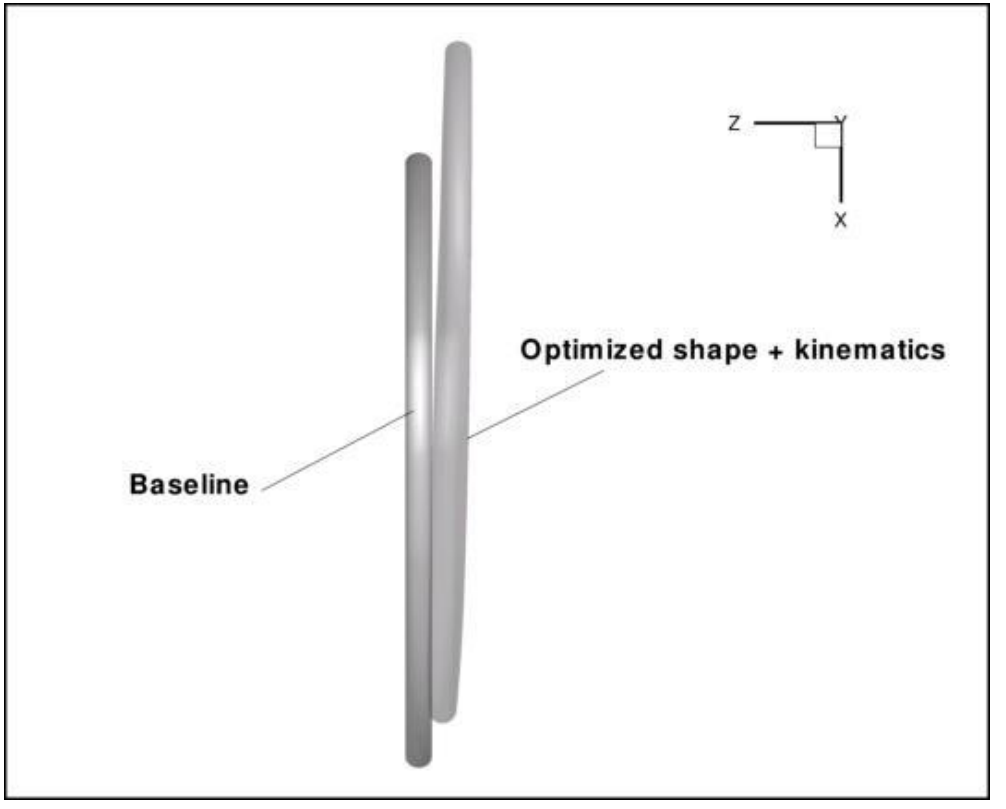

Baseline and optimized wing geometries

Combined Optimization of wing shape and kinematics (cont.)

Baseline **Optimal**

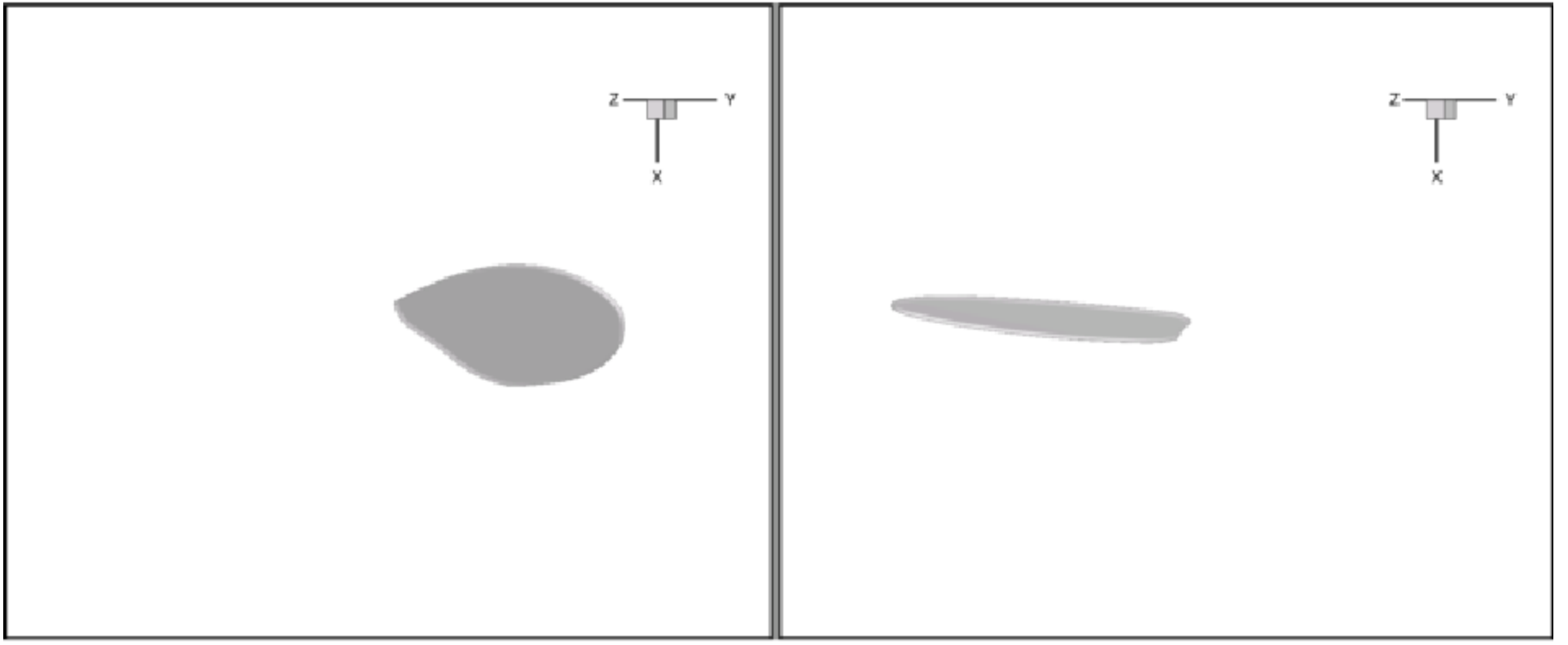

The baseline (left) and optimized wing kinematics.

Combined Optimization of wing shape and kinematics (cont.)

Baseline **Optimal**

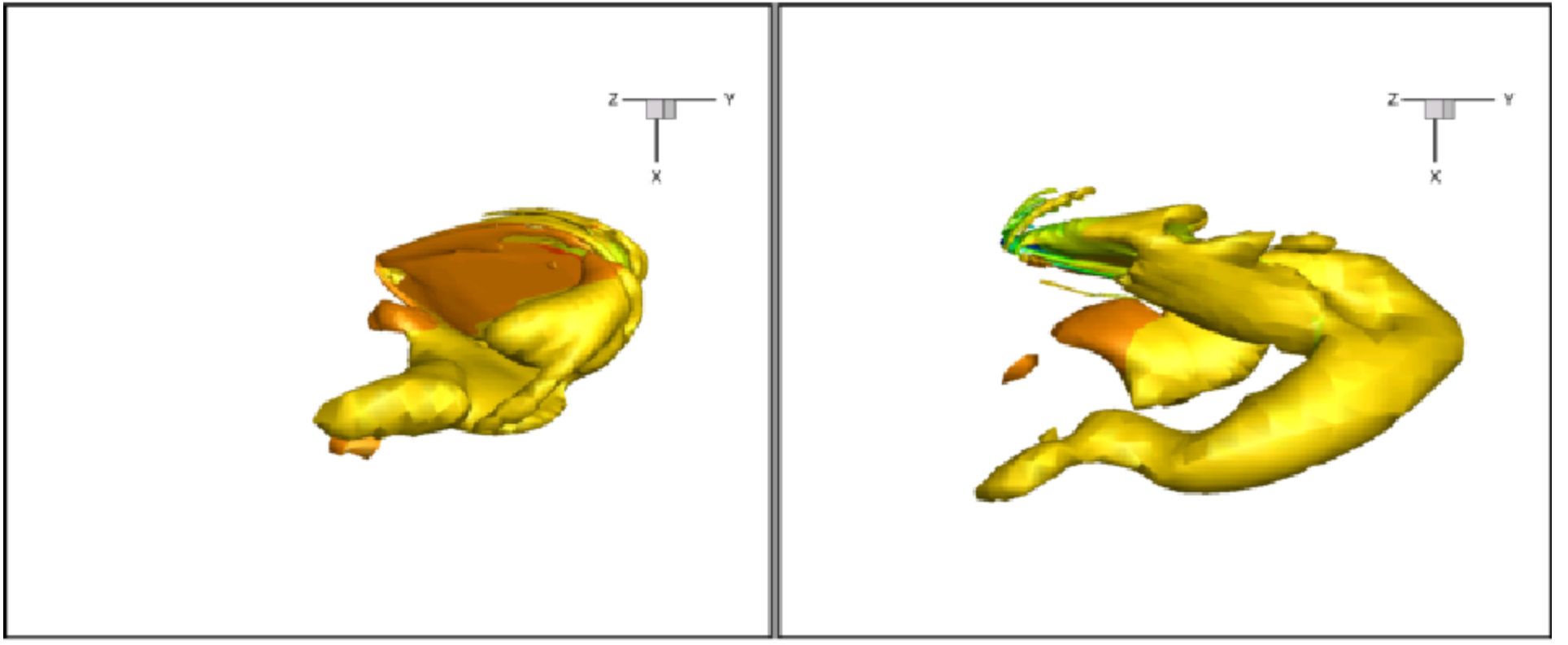

Iso-surface of the *q*-criterion colored with pressure contours obtained with the baseline (left) and optimized wing shape and kinematics.

Combined Optimization of wing shape and kinematics (cont.)

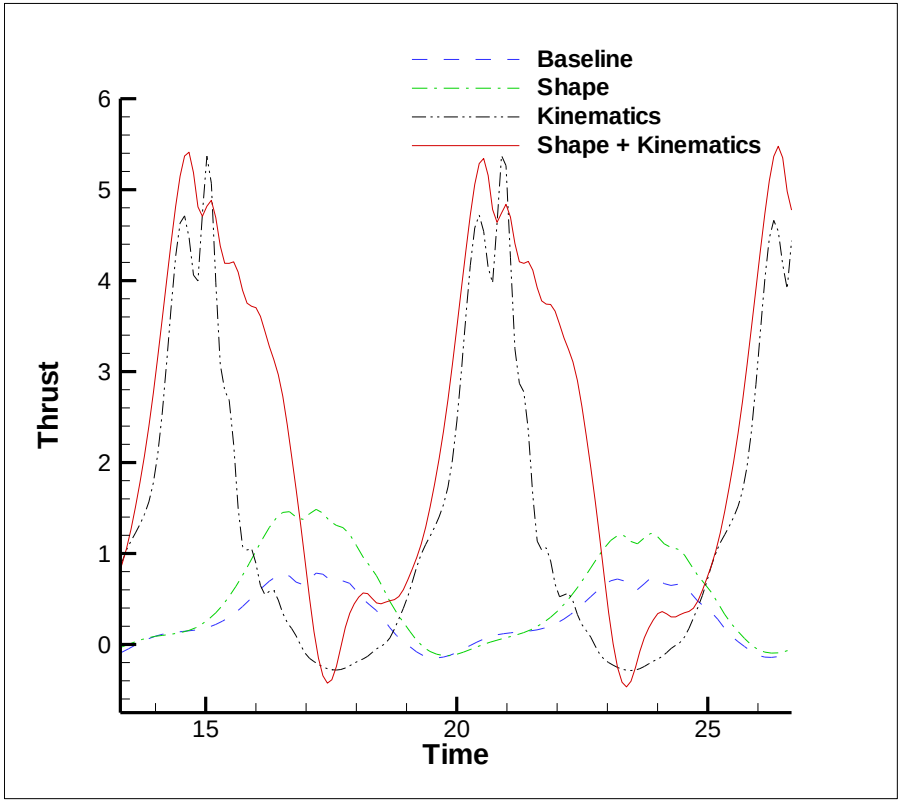

Baseline and optimized thrust coefficients.

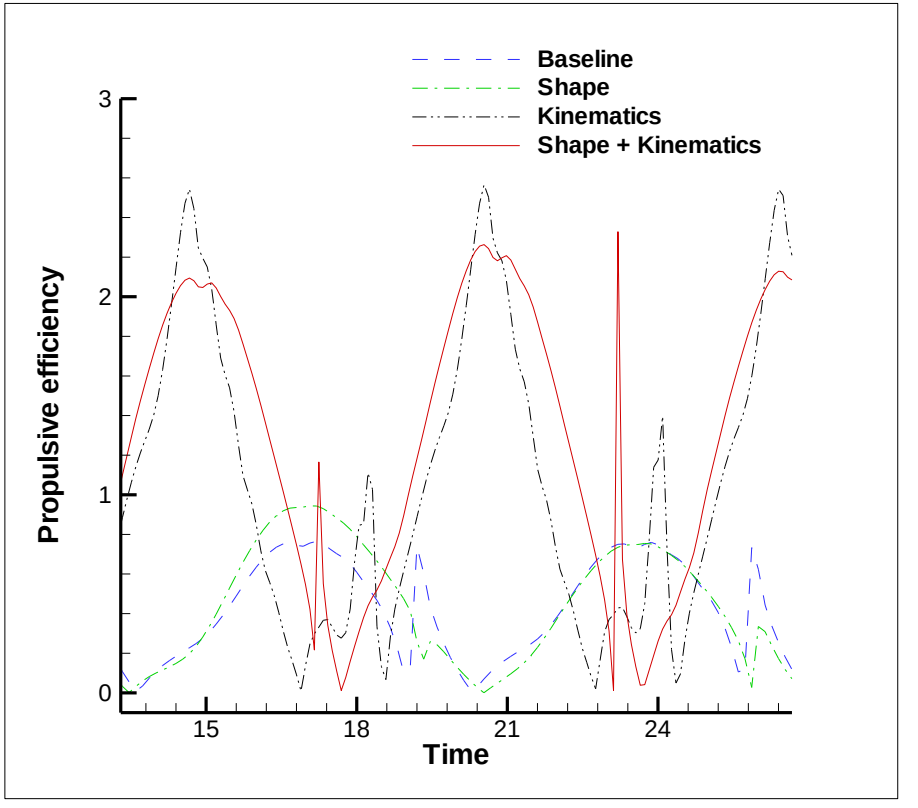

Propulsive efficiency before and after optimization.

Combined Optimization of wing shape and kinematics (cont.)

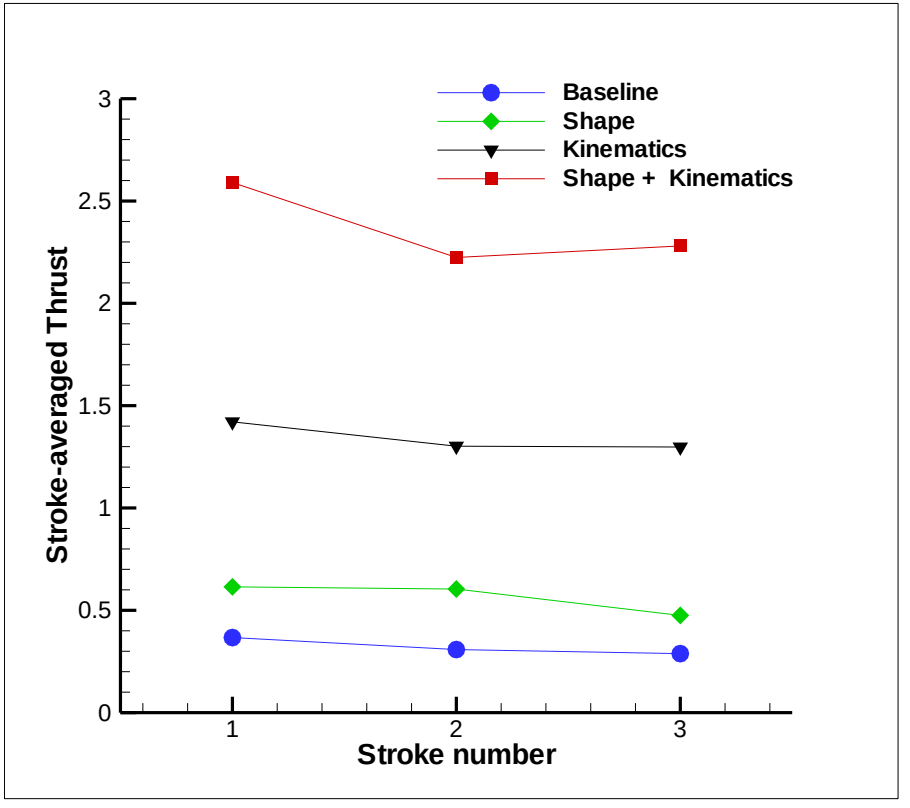

Stroke-averaged thrust coefficients

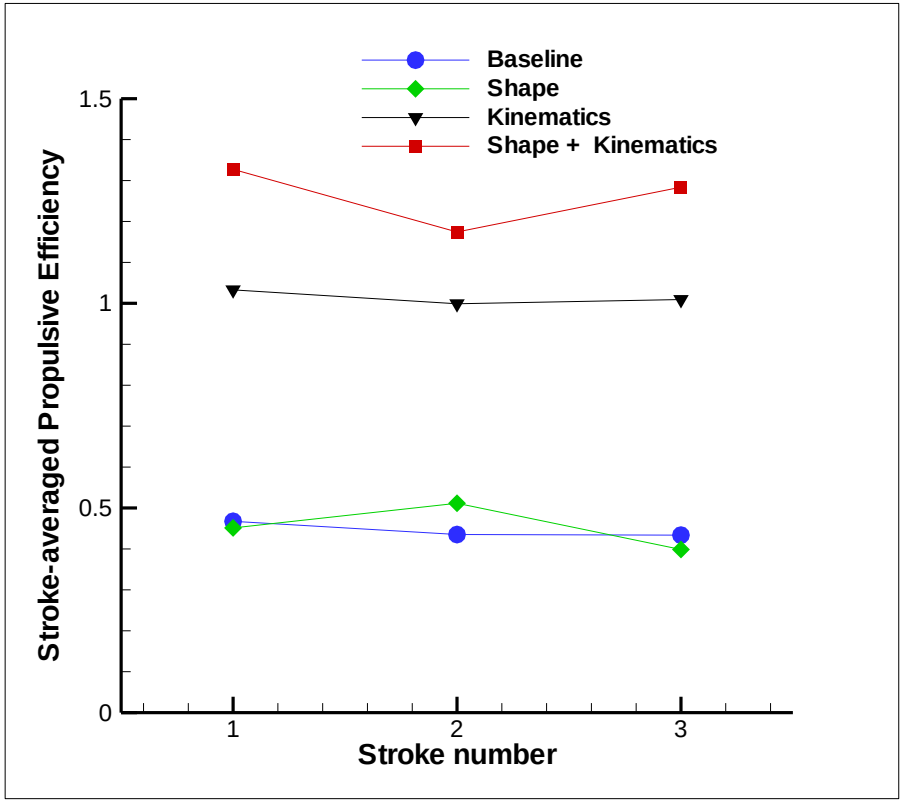

Stroke-averaged propulsive efficiency

Validation of Optimization Results

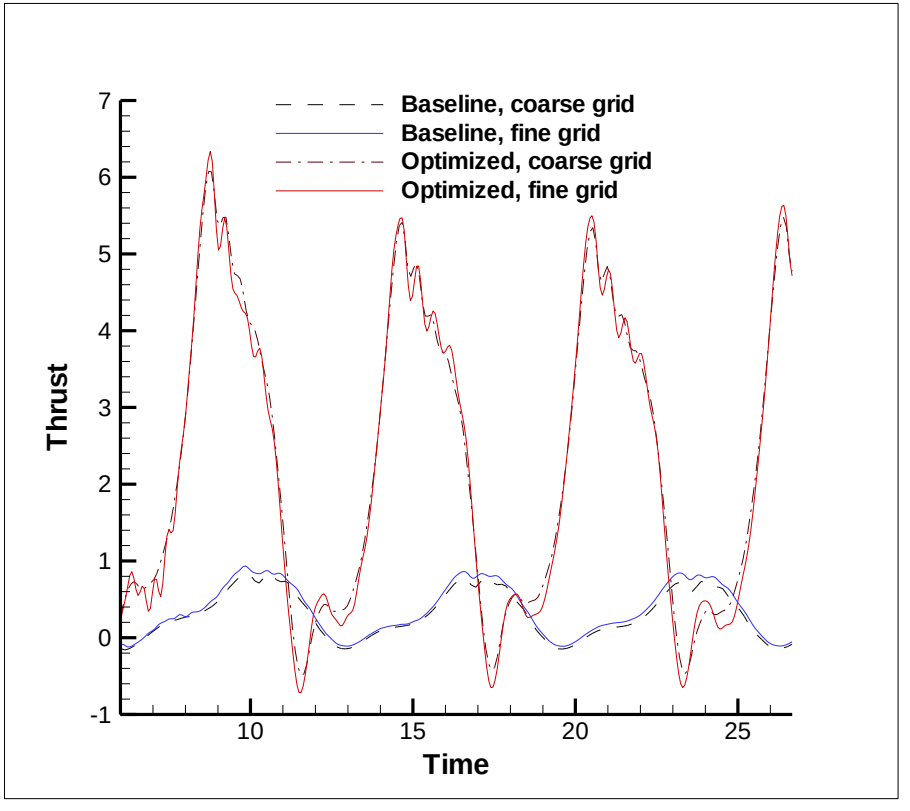

Thrust coefficients computed on coarse and fine grids.

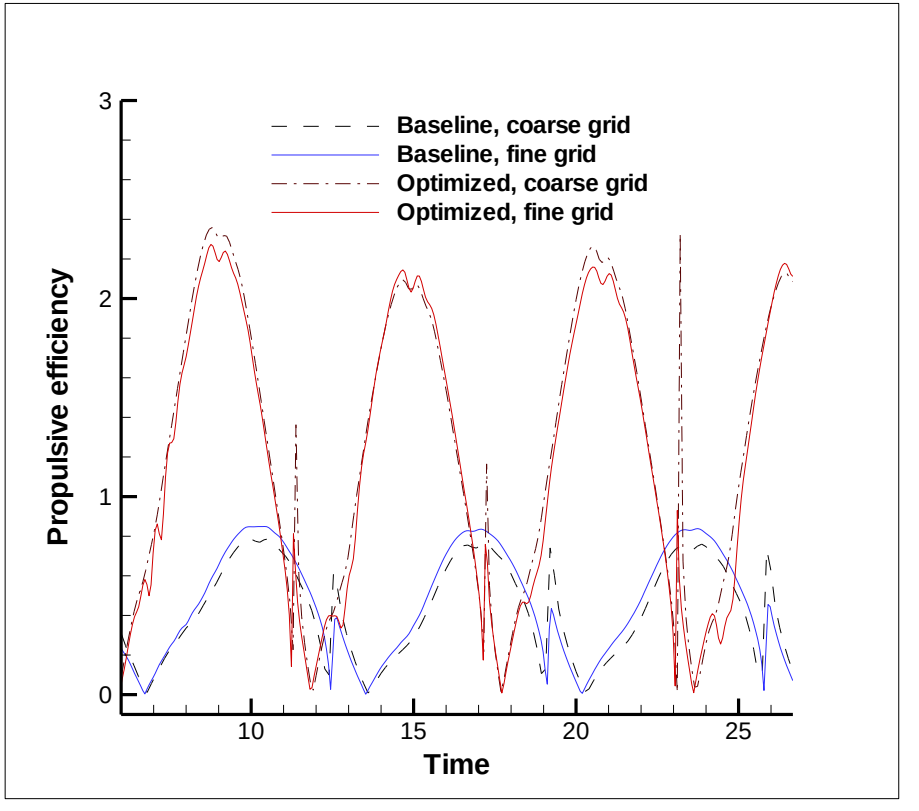

Propulsive efficiency computed on coarse and fine grids

Some observations

Hummingbird

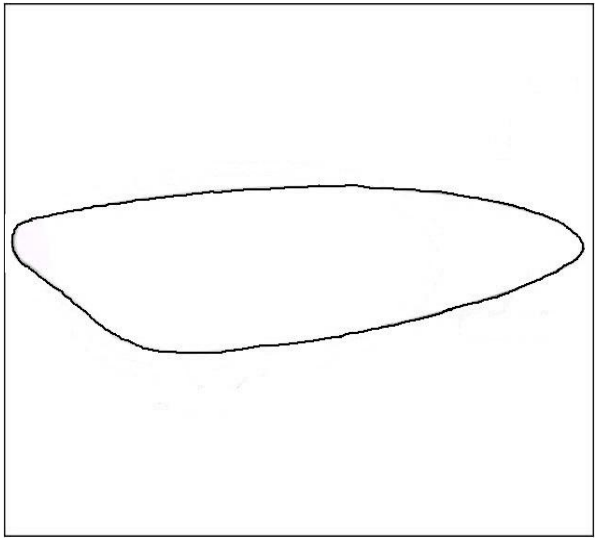

Wing obtained by optimization of wing shape

Some observations (cont.)

Wasp wing

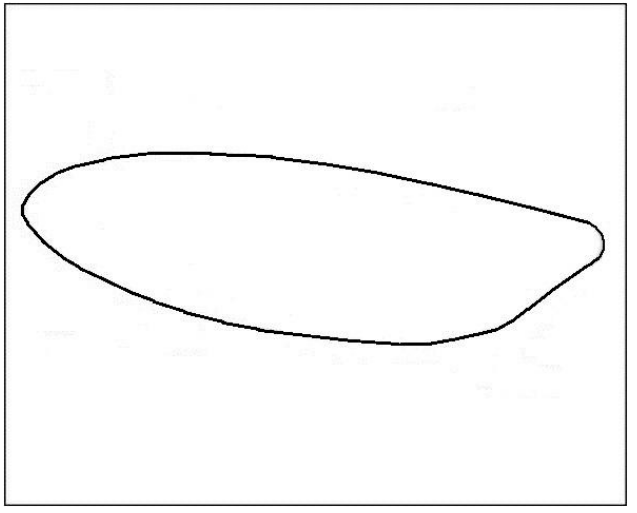

Wing obtained by combined optimization of shape and kinematics

Conclusions

- Optimization of shape, kinematics, and their combination have increased the stroke-averaged thrust coefficient by a factor of 1.6, 3.8 and 6.7, respectively
- The propulsive efficiency has been increased by a factor 1.05, 2.4, and 2.9, respectively.
- The wing span and aspect ratio have been significantly increased after optimization.
- Stroke, pitch and heave angle amplitudes have also been significantly increased.
- The wing twist have no appreciable effect on the thrust and propulsive efficiency.
- The optimized wing tip stroke path closely resembles a figure-eight shape observed in flying insects.
- All these factors considerably increase the size and strength of the leading and trailing edge vortices.
- The combined optimization of wing shape and kinematics provides the highest increase in thrust and PE, which cannot be achieved using shape or kinematics optimization alone.
- Optimal wing shape and kinematics resemble those observed in flying insects.

Future Directions

- Adjoint-based optimization of a two-wing MAV.
- Use the adjoint method to improve the MAV controllability.
- Multipoint optimization including various flight scenarios, such as hover, forward flight, maneuvering, wind gust mitigation, etc..
- Include transition prediction and aeroelasticity into the adjoint-based optimization framework

Questions?